Identification of a new inhibitor of Ran GTPase with potential therapeutic value in epithelial ovarian cancer

Zied Boudhraa[δ,1,2], Xiaohong Tian[δ,3], Ryhem Gam[ξ,1,2], Sabrina Ritch[ξ,1,2], Jennifer Kendall-Dupont[1,2], Euridice Carmona[1,2], Diane Provencher[1,2,4], Jian Hui Wu[3], Anne-Marie Mes-Masson[1,2,5*]

[1] Centre de recherche du Centre hospitalier de l'Université de Montréal (CRCHUM), Montreal, Canada.

[2] Institut du cancer de Montréal (ICM), Montreal, Canada.

[3] Lady Davis Institute, Jewish General Hospital, McGill University, Montreal, Canada.

[4] Division of Gynecologic Oncology, Université de Montréal, Montreal, Canada.

[5] Department of Medicine, Université de Montréal, Montreal, Canada.

[δ] First Co-authors

[ξ] Second Co-authors

[*] **Corresponding author:** Anne-Marie Mes-Masson, CRCHUM, R10-412, 900 rue St-Denis, Montreal, Quebec, Canada, H2X 0A9. Phone: (514) 890-8000 ext. 25496. E-mail: anne-marie.mes-masson@umontreal.ca

ABSTRACT

Compiled research studies suggest that the small GTPase Ran is critical in cancer initiation and progression. Compounds that block Ran activity would be valuable for cancer treatment. Yet, to date, there is no inhibitor proven to be efficient and specific to Ran. Here, by learning lessons from the discovery of KRAS G12C inhibitors, we generated a structural model of the switch II pocket of GDP-bound Ran to identify potential inhibitors of Ran by virtual screening. After *in vitro* verification, compound M26 was detected. Subsequent hit optimization lead us to identify compound M36 as an inhibitor of Ran with a promising therapeutic value. Binding of M36 to Ran was confirmed by cellular thermal shift assay. The specificity of M36 towards Ran was demonstrated by the evaluation of the active GTP-bound forms of a range of GTPases including Ran, RhoA, Cdc42 and Rac1; and by the expression of a dominant active mutant of Ran. Remarkably, similar to depletion of Ran by siRNA, M36 exhibits a specific toxicity in aneuploid ovarian cancer cells and represses DNA repair systems. In accordance with this, we demonstrated a synergistic relationship between M36 and the FDA approved PARP inhibitor Olaparib. *In vivo*, M36 presents acceptable pharmacokinetic properties and, more importantly, inhibits the tumor growth of an aggressive epithelial ovarian cancer xenograft model. Clinically relevant, M36 was able to induce cell death in *ex vivo* EOC patient derived micro-dissected tumor. Overall, our study is the first to provide a small-molecule compound inhibitor of Ran with a promising therapeutic potential.

INTRODUCTION

Ran (Ras related nuclear protein), a member of the RAS superfamily of small GTPases, is unique among other GTPases owing to its cellular localization. While other GTPases are found in the cytoplasm and associated to cellular membranes, Ran is found predominately in the nucleus [1]. Ran has been widely studied for its role in mitosis and nucleo-cytoplasmic shuttling of proteins and RNAs [2]. In comparison with normal tissues, Ran was found to be overexpressed in several cancers including breast, renal, gastric, colon, pancreatic, ovarian and lung cancers [3-10]. Furthermore, within the same cancer, the expression of Ran has been found to be positively correlated with patient outcomes in myeloma, lymphoma, neuroblastoma, renal cell, ovarian and breast carcinomas [4-6,10-14]. It has been reported that Ran is involved in supporting at least three hallmarks of cancer, namely proliferative signaling, resisting cell death and activating pathways that support invasion and metastasis [7,9,11,15-17]. Interestingly, we and others have been reported that the loss of Ran using specific siRNAs is lethal for cancer cells with no or moderate effect in normal cells [7,18-21]. This suggests that targeting Ran could achieve a valuable therapeutic index.

Epithelial ovarian cancer (EOC) is the most common form of all ovarian cancers and is the most fatal of all gynecological malignancies [22,23]. Histologically, EOCs are subdivided into five subtypes where the high-grade serous carcinoma (HGSC) is overrepresented and rates among the most aggressive [22,24]. EOCs are characterized by extremely high intratumoral heterogeneity that poses specific challenges for therapeutic strategies [24,25]. However, despite this heterogeneity, aneuploidy is a hallmark of EOC, particularly of HGSC [26] where the chromosomal stability control gene, *TP53*, is mutated in >90% of cases [27,28]. Thus, targeting aneuploidy could potentially treat this cancer.

43 Recently, we have shown, using EOC models, that the differential sensitivity between
44 normal and cancer cells following the loss of Ran is governed by aneuploidy and genomic
45 instability [19]. In particular, we have reported that induction of aneuploidy in rare diploid EOC
46 cell lines or normal cells renders them highly dependent on Ran. We also established an inverse
47 correlation between Ran and the tumor suppressor NR1D1 and reveal the critical role of
48 Ran/NR1D1 axis in aneuploidy-associated endogenous DNA damage repair. We showed that
49 Ran, through the maturation of miR4472, destabilizes the mRNA of NR1D1 impacting several
50 DNA repair pathways [19]. Loss of Ran was then associated with NR1D1 induction, accumulation
51 of DNA damages and lethality of aneuploid EOC cells. Our findings suggest a synthetic lethal
52 strategy targeting aneuploid cells based on their dependency to Ran. We hypothesize that
53 developing small molecules targeting this GTPase is an attractive therapeutic approach for EOC.
54 To date, despite the availability of Ran's crystal structure [29-33], there is no inhibitor proven to be
55 efficient and specific to Ran. The high affinity of Ran to its cognate GTP (pM range) and the
56 high cellular concentration of GTP (millimolar range), makes the identification of an efficient
57 compound with a GTP-competitive mode of action very difficult, if not impossible.

58 In the present study, inspired by the ground-breaking work of KRAS G12C inhibitors
59 [34,35], we aimed to identify allosteric small molecule inhibitors of Ran. The approach chosen was
60 to target the GDP-bound form of Ran at the switch II pocket, with the hypothesis that this would
61 lock the protein in an inactive state, thereby depleting the active Ran population. To this end, a
62 part of the NCI chemical database (90,000 compounds) was screened virtually. After *in vitro*
63 validation and hit optimization, we identified M36 as a promising inhibitor of Ran. Binding of
64 M36 to Ran was confirmed by cellular thermal shift assay. M36 mimics the effect of Ran knock
65 down (KD): specific toxicity in aneuploid cancer cells and significant repression of the DNA

damage repair (DDR) process. *In vivo*, M36 is well tolerated by mice at high doses, displays an acceptable pharmacokinetic (PK) pattern and significantly delays tumor growth of a very aggressive EOC xenograft model. At the clinical level, M36 was able to induce cell death in *ex vivo* micro-dissected tumors derived from an EOC patient. Furthermore, owing to its ability to repress DNA repair systems, we established a synergistic relationship between M36 and the FDA approved PARP inhibitor Olaparib. Overall, our findings suggest a new therapeutic strategy for EOC based on the modulation of Ran in aneuploid cells.

RESULTS

In silico and cell-based screenings identified M26 as hit compound for Ran inhibition

Inspired by the ground-breaking work of KRAS G12C inhibitors, which bind KRAS G12C mutant at a pocket nearby switch II (referred to as switch II pocket) [34,35], we aimed to target the GDP-bound form of Ran (RanGDP) at the switch II pocket to 'arrest' Ran at its inactivated state (**Figure 1A**). However, one key feature of the switch II pocket of KRAS G12C is that it exists only when it binds with an inhibitor. Our inspection of the crystal structure of RanGDP (pdb: 3ch5) found no pre-formed switch II pocket. We thus decided to construct a structural model of the switch II pocket of RanGDP using the crystal structure of KRAS G12C/Inhibitor complex (pdb: 5v6s) as the template **(Figure 1A)**. Next, a part of the NCI chemical database (90,000 compounds) was screened virtually against the RanGDP switch II pocket. Top-ranking compounds identified in this *in silico* screen went through a more in-depth visual inspection for binding modes. A total of 28 compounds were selected for further study as potential Ran inhibitors (**Figures 1B and S1A**). Having previously established that aneuploid EOC cells are more sensitive to the loss of Ran than normal or tumoral diploid cells [19], biological activity was

89 assessed by clonogenic assays (at a single dose of 10 μM) using one aneuploid EOC cell line
90 (TOV112D) and the diploid normal ARPE (ARPE-19) cells **(Figures 1C and S1B)**. The
91 criterion for a positive hit was that the compound did not inhibit the colony formation of the
92 ARPE cells but significantly inhibited the number of colonies formed by the TOV112D cells.
93 Our results show that one compound from the *in silico* screening, M26 **(Figure 1B)**, inhibited
94 colony formation of EOC but not the normal cells **(Figure 1C)**. Furthermore, by analyzing
95 PARP cleavage by Western blot, we found that M26 treatment induced apoptosis in TOV112D
96 cells with no notable effect in ARPE cells **(Figure 1D)**, indicating a differential sensitivity
97 between the diploid and aneuploid cells following M26 treatment. Since our screening was
98 virtual using Ran crystal structure, it was therefore important to determine whether our hit
99 compound was able to inhibit Ran in its biological form. For that, the level of active GTP-bound
100 Ran was evaluated in lysates of EOC cells treated or not with M26 using Ran pull down assays.
101 Because of the fast turnover between Ran-GTP and Ran-GDP, a fast incubation time (1 h) and a
102 higher compound concentration is recommended for this pull down assay, as described in
103 previous publications regarding other GTPases, such as RalA [36]. Our results showed a marked
104 decrease in Ran-GTP level in TOV112D cells incubated with M26 compared to DMSO-treated
105 control cells **(Figure 1E)**. Collectively, our data identified M26 as a potential inhibitor of Ran
106 with an interesting therapeutic value.

107 **Chemical optimization and cell-based screening identified M36 as a more promising**
108 **inhibitor of Ran**

109 Plasma esterases are the major drug-metabolizing enzymes in plasma significantly affecting drug
110 stability *in vivo* [37]. As shown in **Figure 1B**, M26 has three ester groups, which would suggest
111 poor bioavailability of the drug when injected *in vivo*. To overcome this issue and explore

112 preliminary structure-activity relationship, a series of M26-derived compounds, in which the
113 ester groups were replaced by ether groups, were synthetized **(Figures 2A and S2A)**. Our results
114 showed that only compound M36 and its derivative M98, inhibited colony formation of
115 TOV112D cells without affecting the ARPE cells **(Figure S2B)**. Interestingly, M36 but not M33
116 inhibited the activation of Ran comparably to the parent compound, M26 **(Figure S2C)**.
117 Therefore, for the rest of the study we selected M36 **(Figure 2A)** for further characterization.
118 Using Ran pull down assays, the effect of M36 on Ran activation was shown to be dose
119 dependent **(Figure 2B)**. In addition, immunofluorescence studies using an antibody specific to
120 active Ran-GTP showed no detectable levels of Ran-GTP in TOV112D cells treated with M36 as
121 compared to the intense staining of the DMSO-treated cells **(Figure 2C)**. More importantly, the
122 direct binding of M36 to RanGTPase was assessed by cellular thermal shift assay (CETSA), a
123 widely used technique to verify the interaction of a compound with its target protein [38]. In this
124 assay, the thermal stability of Ran was investigated at different temperatures in OV1946 cells
125 treated with different concentrations of M36 or with DMSO **(Figures S3A-B)**. Like the pull
126 down assay, shorter incubation time (1 h) and higher compound concentrations are needed for
127 CETSA in order to detect binding of no-covalent interactions. As expected, Ran levels detected
128 by Western-blot decreased with increasing temperatures in controls cells treated with vehicle
129 DMSO. However, a shift in this thermal instability was observed when cells were treated with
130 M36, specially at the concentrations of 100 and 200 μM. Significantly higher levels of Ran were
131 observed at all M36 concentrations for temperatures of 58°C, 59°C and 60°C **(Figure S3A)**,
132 indicating M36 engages with Ran and increases its thermal stability. As negative control, we
133 show that this protection was not observed when OV1946 cells were treated with the same
134 increasing concentrations (50-200 μM) of the PARP inhibitor Olaparib (**Figure S3C**), a drug

135 known to impact DNA repair [39]. Since this CETSA relies on densitometry analyses of Western
136 blot bands, we confirmed these results with the more quantitative HiBiT CETSA [40]. This method
137 uses a commercially available luminescent tag (HiBiT from Promega) for protein thermal
138 stability assessment. Here, OV1946 cells were transiently transfected for 24 h with Ran cDNA
139 having N-terminal HiBiT tag (see Methods for details), treated with 100 μM M36 or DMSO for
140 1 h, and heated for 3 min at different temperatures. Luminescence from the HiBiT tag was then
141 measured in cell lysates. As expected luminescence signal decreased with increasing
142 temperatures, and a shift in this thermal stability was observed when cells were treated with M36
143 when compared to DMSO treated cells (**Figure 2D**). Significant differences were observed at
144 temperatures from 57°C to 62°C, corroborating the CETSA results using Western blot. Overall,
145 these results indicate that M36 targets Ran and inhibits Ran-GTP activation.

146 Regarding its effect on cancer cells, the IC_{50} value of M36 for the TOV112D cell line as
147 determined by clonogenic assay was found to be 10.02±0.36 μM. Only a minimal effect was
148 observed for the normal ARPE cell line at high concentrations **(Figure 3A)**. To support our
149 observation regarding the differential sensitivity between diploid and aneuploid cells with M36
150 treatment, we expanded our analysis by using, in addition to ARPE and TOV112D cell lines, five
151 aneuploid HGSC cell lines [TOV1946, TOV2295(R), OV1946, OV866(2) and OV4485] and one
152 diploid low-grade serous EOC TOV81D cell line. Proliferation assays were performed on these
153 cell lines after treatment with M36 and a concentration higher than the observed IC_{50} value was
154 chosen (40 μM) to better evaluate differential effects. As a positive control, the same cell lines
155 were transfected with siRan that we have previously characterized for its specificity [19,41].
156 Remarkably, like siRan, M36 demonstrated a specific toxicity in aneuploid cells with only a
157 moderate effect in normal and EOC diploid cells **(Figure 3B)**. Similarly, this toxicity was

158 accompanied by the induction of apoptosis specifically in aneuploid cells **(Figure 3C)**,
159 highlighting the therapeutic potential of M36. Since aneuploidy and genomic instability are
160 hallmarks of the majority of cancers [42,43], we assessed the toxicity of M36 in other cancer cell
161 lines derived from prostate, gastrointestinal, breast and skin cancers. Strikingly, M36 showed a
162 significant toxicity in all the cell lines tested **(Figure S4A)**. These results suggest that the use of
163 M36 would not be limited to ovarian cancer but could be extended to other tumors. To
164 investigate the specificity of M36 towards Ran, the effect of M36 on the activation of other
165 GTPases (RhoA, Cdc42 and Rac1) was assessed. As shown in **Figure 3D**, no decrease in the
166 activation of these GTPases was observed when incubated with M36. In corroboration, no
167 thermal stability of Cdc42 was observed on CETSA after M36 treatment **(Figure S3D)**.
168 Furthermore, overexpression of constitutively active (GTP-bound form) Ran^{Q69L} mutant protein
169 [44] mitigated the inhibition of TOV112D cell growth by M36, whereas overexpression of
170 dominant negative Ran^{T24A} mutant [44] had similar effect as the wild-type (WT) protein **(Figure**
171 **3E)**. Furthermore, HiBiT CETSA experiments performed at 59°C in OV1946 cells show that
172 M36 was able to protect Ran WT and Ran^{T24A}, but not Ran^{Q69L}, from thermal instability **(Figure**
173 **2E)**, suggesting that M36 does not bind to the GTP-bound form of Ran. Together, these data
174 provide evidence of the specificity of M36 towards Ran and indicate that this compound acts
175 specifically on the GDP-bound form of Ran.

176 **M36 mimics the effect of Ran knock down (KD) regarding DDR**

177 We have shown that the differential sensitivity between diploid and aneuploid cells following the
178 loss of Ran comes from the involvement of the Ran/NR1D1 axis in modulating DNA repair [19]. In
179 fact, following the loss of Ran, NR1D1 was induced and in turn repressed several DNA repair
180 pathways including the homologous recombination (HR) and the non-homologous end joining

181 (NHEJ) pathways, leading to the accumulation of DNA damages. We first assessed the effect of
182 M36 on NR1D1 expression. As observed following Ran KD, M36 significantly induced the
183 expression of NR1D1 in two aneuploid EOC cell lines (TOV112D and OV1946) **(Figure 4A-B)**.
184 As negative control, we have shown that NR1D1 expression was not affected when cells were
185 treated with the PARP inhibitor Olaparib **(Figure S4B)**, suggesting that M36 effect on NR1D1
186 expression is specific. Next, to investigate whether M36 was able to repress the DDR process,
187 TOV112D cells were either transfected with siRan or treated with M36 and the DDR
188 components were analyzed by immunofluorescence. Remarkably, in accordance with Ran KD,
189 M36 treatment induced DNA damage accumulation as shown by an increase of p-γH2AX foci
190 number **(Figure 4C)** and an inhibition of the HR and the NHEJ pathways, which were assessed
191 respectively by the quantification of Rad51 **(Figure 4D)** and 53BP1 **(Figure 4E)** foci formation.
192 Interestingly, since the cytoplasmic staining of 53BP1 following M36 treatment was increased
193 **(Figure 4F)**, the inhibition of 53BP1 foci formation by M36 can probably be attributed to the
194 inhibition of the Ran-dependent nuclear import of this protein that has been previously reported
195 [15] and is in accordance with the Ran KD condition **(Figure 4F)**. Collectively, our data
196 demonstrate that M36 mimics the effect of the loss of Ran regarding DDR.

197 **Evaluation of the therapeutic potential of M36 *in vivo***

198 The promising *in vitro* results of M36 led us to initiate *in vivo* analysis of this small molecule
199 inhibitor of Ran. PK results showed that after a single intraperitoneal (IP) injection (200 mg/kg),
200 plasma levels of M36 was detected at our first time point of 5 minutes, reached a peak at 30
201 minutes (100 μM), remained at around 10 μM after 6 h and is still detectable at 24 h **(Figure**
202 **5A)**. Therefore, M36 displayed an acceptable PK pattern. For the tolerance study, M36 was
203 injected IP daily for a period of three weeks. Our results showed that treated mice continued to

204 gain weight **(Figure 5B)**, suggesting that, even at higher doses (200 mg/kg), M36 was well
205 tolerated. Inhibition of tumor growth was evaluated in the human chemoresistant EOC xenograft
206 model, TOV112D. As we've previously shown, this xenograft model showed resistance to
207 carboplatin treatment [45]. Furthermore, when mice were treated with the maximum tolerated dose
208 of the PARP inhibitor Olaparib **(Figure 5C)**, no significant effect was observed regarding tumor
209 growth. However, M36 treatment significantly delayed tumor growth of this aggressive model
210 **(Figure 5D-E)** and prolonged mouse survival **(Figure 5F)**, highlighting the promising potential
211 of this compound for the treatment of EOCs, particularly for patients with poor prognosis.

212 **M36 induces cell death in *ex vivo* ovarian cancer models**

213 To evaluate the clinical relevance of M36 treatment, the viability of microdissected tumor
214 samples derived from EOC xenografts or from a patient tumor were evaluated *ex vivo* using our
215 microfluidic methodology [46]. Our results show **(Figure 6)** a significant increase in the intensity
216 of cleaved caspase 3 (CC3) staining 72 h after M36 treatment in both the OV1946 xenograft and
217 the TOV12018G patient tumor models. For the TOV112D xenograft model, this effect was also
218 observed, but no significance was achieved **(Figure S4C)**, and a 50% decrease in the nuclear Ki-
219 67 staining was observed in this model 24 h post-treatment. These results suggest that M36
220 induces cell death by apoptosis and could decrease cell proliferation in *ex vivo* EOC models,
221 including patient tumor, further corroborating its potential therapeutic value.

222 **Combination of M36 and Olaparib triggers synthetic lethality in EOC cells**

223 It is presumed that resistance to PARP inhibitor therapy is closely related to the activation of the
224 HR pathway of cancer cells [47]. Therefore, combination treatments of PARP inhibitor with drugs
225 that inhibit the HR pathway would be promising to circumvent this resistance. Based on our

226 finding that M36 was able to repress the HR pathway, we sought to determine whether M36 was
227 able to sensitize EOC cells to Olaparib. First, we investigated the effect of M36 on the activation
228 of the HR pathway by Olaparib. Our data in two HR proficient BRCA1/2 WT EOC cell lines
229 [TOV112D, OV866(2)] showed that M36 pre-treatment efficiently inhibited the induction of the
230 HR pathway (assessed by Rad51 foci quantification) by Olaparib **(Figure 7A)**, and this
231 repression was comparable when irradiation was used as an inducer of this DNA repair pathway
232 **(Figure 4D)**. Next, combination treatments of M36 with Olaparib were undertaken in three
233 BRCA1/2 WT and Olaparib resistant-cell lines, namely TOV112D, OV866(2) and OV90 cell
234 lines, together with the normal diploid ARPE cell line. These combinations were performed
235 using increasing concentrations of both drugs (all concentrations used are below the IC_{50}) and
236 evaluated using the Bliss independent model [48], in which values below -1 indicate antagonism,
237 values between -1 and 1 indicate additive effects and values above 1 indicate synergy.
238 Remarkably, in contrast to ARPE cells that did not respond to any combination condition, M36
239 displayed a potent synergistic interaction with Olaparib in all 3 EOC cell lines (Bliss scores
240 ranging from 41.02 to 78.6) **(Figure 7B-D)**. Similarly, while no effect was observed in ARPE
241 cells, M36/Olaparib combination induced a significant increase of cell death in the EOC cell
242 lines in comparison with single treatments, as assessed by FACS using DRAQ7 staining **(Figure
243 7E)** and by Western blot using cleaved caspase-3 antibody **(Figure 7F)**. Overall, our data
244 indicate that combining M36 with Olaparib would be an effective combination therapy to
245 counter PARP inhibitor resistance in ovarian cancer.

246 In all, we describe here a first-in-class small molecule inhibitor of the Ran GTPase targeting
247 aneuploid EOC. However, further medicinal chemistry is needed to improve potency and
248 compound solubility, and we are aware that M36 is not ultimate inhibitor to go forward to a

clinical setting. Using the computational model proposed and the M36 scaffold, we are confident that better compounds targeting the Ran GTPase could be unraveled in a near future.

DISCUSSION

The involvement of Ran GTPase in cancer initiation and progression has been discussed for more than a decade [7,8,15,17,21,41,49-51]. Furthermore, using several *in vitro* and *in vivo* experimental models, Ran has been proposed as a promising therapeutic target of cancer [8,9,14,17-19,52]. Recent reports have proposed new strategies to target Ran in the context of cancer therapy. One of them relies on repurposing Pimozide in Ran Targeting [53]. Pimozide was initially identified as a potent antagonist of dopamine receptor D2 (D2R) and used as an antipsychotic drug for the management of schizophrenia and other psychotic disorders. It has been shown that Pimozide inhibits the expression of Ran at the transcriptional level and inhibits breast cancer cell growth *in vitro* and *in vivo* [53]. Although this molecule displays an interesting cancer therapeutic value, it is likely that this drug will display severe side effects at the concentrations needed. In fact, it has been shown that mice lacking D2R had impaired motor activity and movement coordination as well as hyperactivity [54]. More importantly, the dosage of Pimozide for patients with psychotic disorders is about 0.2 mg/Kg/day, however, in the *in vivo* study proposed for breast cancer therapy, mice were treated daily with Pimozide at 20 mg/Kg/day in order to have a significant effect on tumor growth [53]. These very high doses of Pimozide will inevitably be an issue in the exploration of this drug in the context of cancer. Another strategy relies on Nano-encapsulation technology (using PLGA-based nanoparticles) of a shRNA targeting Ran [55] or a peptide inhibiting the activation of this GTPase by disrupting the interaction between Ran and RCC1 [56,57]. Such an approach presents many obstacles making its use in clinic very difficult. First, upon

272 entering the circulation, nanoparticles (NPs) are often coated with opsonin proteins leading to
273 their clearance by macrophages and affecting their pharmacokinetic properties [58]. Second, blood
274 vessels are leaky with fenestrations ranging between 0.2 and 1.2 μm. Since NPs exist in a range
275 of sizes, it is thought that the size of therapeutic NPs should be well below 200 nm [58,59].
276 However, the NPs used for Ran targeting have a mean diameter of 182–277 nm [56].

277 Here, we aimed to target Ran directly with a new small molecule inhibitor. To date, there
278 is no available drug specific to Ran. One reason for this is the high intracellular concentration of
279 GTP as well as the high affinity of GTP to its cognate GTPase, making the development of an
280 efficient competitor of GTP difficult. Alternatively, it is thought that developing allosteric
281 compounds able to interact with a given GTPase in its GDP-bound form and to lock it on its
282 inactive state is more relevant to attenuate GTPase activity. Inspired by the work of KRAS G12C
283 inhibitors, which bind KRAS G12C mutant at the switch II pocket [34,35], we aimed to target the
284 RanGDP at the switch II pocket to 'arrest' Ran at its inactivated state. However, our inspection
285 of the crystal structure of RanGDP (pdb: 3ch5) found no pre-formed switch II pocket. We thus
286 constructed a structural model of RanGDP switch II pocket by homology modeling and
287 performed in silico screening against the switch II pocket. Chemical optimization of our initial
288 hit M26 lead to compound M36 as a novel Ran inhibitor. Importantly, M36 displays, *in vitro,* a
289 very interesting therapeutic index between normal/diploid and cancer/aneuploid cells that is in
290 alignment with our *in vivo* data. In fact, at higher doses, M36 is well tolerated by mice and
291 exhibits a significant toxicity for one of the most aggressive xenograft models, TOV112D, that
292 do not respond to conventional treatments such as Carboplatin or Olaparib therapies.
293 Furthermore, at the clinical level, M36 was able to induce cell death by apoptosis in *ex vivo*
294 micro-dissected tumors derived from an EOC patient. Another advantage of allosteric inhibitors

295 is that they bind to less conserved sites across GTPases and kinases ensuring specificity and
296 avoiding potential severe side effects [60]. In this regard, we have shown that M36 does not
297 influence the activation of other GTPases such as RhoA, Cdc42 and Rac1. More importantly,
298 overexpression of a dominant active of Ran rescued the toxicity of M36 highlighting the
299 specificity of our Ran inhibitor.

300 Olaparib has changed the paradigm for HGSC treatment and has been approved by the
301 FDA as maintenance therapy for patients harboring BRCA1/2 mutations (HR deficient) [61]. This
302 stratification comes from the observation that HR activation is closely linked to non-
303 responsiveness and resistance to PARP inhibitor therapy [47]. Therefore, combination treatment of
304 a PARP inhibitor with drugs that inhibit the HR pathway is actively being exploited in the
305 clinical setting [62,63], and might be effective to induce lethality in HGSC cells. Here, we have
306 shown that M36 induced HR deficiency and dramatically sensitized three BRCA1/2 WT and
307 Olaparib resistant cell lines (TOV112D, OV866(2) and OV90 [64]) to PARP inhibitor therapy.
308 This result is of great interest since it could open new perspectives to circumvent resistance, and
309 possibly to expand PARP inhibitor therapy to patients that are currently excluded. Many cancers
310 are characterized by widespread aneuploidy and genomic instability [42,43]. Hence, targeting these
311 hallmarks would be effective for the development of a new targeted therapy, not only for EOC,
312 but also for a variety of cancers. In our previous work, we have shown that targeting Ran is an
313 effective way to eliminate cancer cells with chromosomal and genomic instability [19]. This
314 prompted us to investigate the therapeutic value of M36 in other cancers. Interestingly, we found
315 that M36 is also toxic in a range of cancer models including prostate, gastrointestinal, breast and
316 skin cancers. These results are encouraging and in future studies we plan to investigate the *in*
317 *vivo* efficacy of M36 in these models.

318 In conclusion, though further medicinal chemistry optimization is required, our study is
319 the first to provide the generation of a first-in-class compound inhibitor of Ran with a therapeutic
320 potential for cancer in general and EOC in particular.
321

322 **METHODS**

323 **Computational modeling and in silico screening**

324 The structural model of RanGDP with switch II pocket was built using crystal structure of
325 RanGDP (pdb: 3ch5) and crystal structure of KRAS G12C in complex with an inhibitor at switch
326 II pocket (pdb: 5v6s) as the templates, by software Modeller (UCSF, CA, USA). Among the 200
327 models generated, the model with lowest objective function was selected for further work.
328 90,000 compounds from NCI-open database were virtually screened against the switch II pocket
329 of the RanGDP model, using software GOLD (The Cambridge Crystallographic Data Centre,
330 Cambridge, UK).

331 **Medicinal chemistry**

332 28 top-ranking candidate compounds were kindly provided, as a gift, by the Drug Synthesis and
333 Chemistry Branch, Developmental Therapeutics Program, NCI, Bethesda, MD, USA. Initial hit
334 M26 was re-synthesized and characterized by NMR analysis. Chemical optimization of M26,
335 leading to compound M36, is described in the supplemental information.

336 **Cell lines and cell culture**

337 The human EOC cell lines used [TOV81D, TOV112D, OV90, OV866(2), TOV1946, OV1946,
338 TOV2295(R), OV4485] were derived in our laboratory from patients' tumors (TOV) or ascites
339 (OV) [65-68]. All EOC cell lines were maintained in low oxygen at 7% O_2 and 5% CO_2 and grown
340 in OSE medium (Wisent, Montreal, QC) supplemented with 10% FBS (Wisent), 0.5 µg/mL

341 amphotericin B (Wisent) and 50 μg/mL gentamicin (Life Technologies Inc., Burlington, ON).
342 The human retinal epithelial cell line ARPE (ARPE-19) was purchased from American Type
343 Culture Collection (ATCC, Manassas, VA) and maintained in DMEM-F12 (Wisent) medium
344 supplemented with 10% FBS (Wisent), 0.5 μg/mL amphotericin B (Wisent) and 50 μg/mL
345 gentamicin (Life Technologies Inc.).

346 **Small interference RNA (siRNA) treatment**

347 Suspensions of 10^6 cells in 100 μL of nucleofector solution V (Lonza Group Ltd, Basel,
348 Switzerland) were transfected by electroporation with 1.2 nmoles siRNA targeting Ran (J-
349 010353-06, ON-TARGETplus, Dharmacon Thermo Fisher Scientific Inc., Waltham, MA). For
350 each experiment, efficiency of Ran silencing was verified 48 hours after transfection by Western
351 blot analysis. Scramble siRNA (D-001810-02, Dharmacon) was used as a control in all
352 experiments.

353 **Clonogenic survival**

354 Clonogenic assays were performed as previously described [64]. Colonies were counted under a
355 stereo microscope and reported as percent of control. IC_{50} values were determined using Graph
356 Pad Prism 5 software (GraphPad Software Inc., San Diego, CA). Each experiment was
357 performed in duplicate and repeated three times. Sensitivity of the cell lines to small molecule
358 inhibitors of Ran was assessed using a concentration range of 0–40 μM.

359 **IncuCyte cell proliferation phase-contrast imaging assay**

360 Cells (2,000 cells/well) were plated in a 96-well plate. The next day, compounds and/or Olaparib
361 (S1060, Cedarlane) were added at the indicated concentrations. Following treatment, cell
362 confluence was imaged by phase contrast using the IncuCyte live cell monitoring system (Essen
363 BioScience, Ann Arbor, MI). Frames were captured at day 0 (immediately after treatment) and at

364 the end of the experiment using a 10X objective. For Ran KD experiments, cells were seeded in
365 a 96-well plate (4,000 cells/well) directly after transfection. Cell confluence monitoring started
366 the next day as described above.

367 **Protein preparation and western blot analysis**

368 Cells were lysed with RIPA buffer containing protease inhibitors. Whole cell lysates were run
369 through a Bradford assay (Thermo Fisher Scientific) for protein quantification. Around 25–50
370 μg of protein was separated by 12.5% SDS-PAGE and transferred onto nitrocellulose
371 membranes. The resultant blots were probed with Ran (1:10 000, sc-271376 Santa Cruz
372 Biotechnology, Dallas, TX), cleaved PARP (1:1000, #9541, Cell Signaling Technology Inc.,
373 Danvers, MA), cleaved caspase 3 (1:1000, #9661, Cell Signaling Technology Inc.), GAPDH
374 (1:2500, #2118, Cell Signaling Technology Inc.) or beta-actin (1:50 000, ab6276, Abcam Inc.,
375 Toronto, ON, Canada) primary antibodies overnight at 4°C then with peroxidase-conjugated
376 secondary antibodies for 2 hours at room temperature. Proteins were detected using enhanced
377 chemiluminescence (Thermo Fisher Scientific).

378 **RT-PCR**

379 The total RNA from TOV-112D or OV1946 cells was isolated using RNeasy Kit (Qiagen®).
380 The total RNA concentration and purity were measured on a NanoDrop™ spectrophotometer.
381 RNA was reverse transcribed using the QuantiTect Reverse Transcription Kit (Qiagen®)
382 according to the manufacturer's protocol. cDNA amplification was performed with SYBR Green
383 PCR master mix (Applied Biosystems®) using the StepOnePlus Real-Time PCR system
384 (Applied Biosystem®). Negative controls were included in all experiments, and actin served as
385 the housekeeping gene. Primers were ordered from Integrated DNA Technologies, Inc:

386 NR1D1:
387 Forward primer: TGGACTCCAACAACAACACAG

388 Reverse primer: GATGGTGGGAAGTAGGTGGG
389 β-actin:
390 Forward primer: CATGTACGTTGCTATCCAGGC
391 Reverse primer: CTCCTTAATGTCACGCACGAT

392 **Cell death analysis by flow cytometry**

393 Cells were treated with M36 and/or Olaparib. Six days after treatment, adherent and floating
394 cells were mixed and incubated 5 minutes at room temperature with DRAQ 7 (ab109202, Abcam
395 Inc). A maximum of 30,000 events were counted per condition using the Fortessa flow cytometer
396 (BD Biosciences, Mississauga, ON) and analyzed with the FlowJo software.

397 **Immunofluorescence**

398 M36 and/or Olaparib-treated and control cells grown on coverslips were washed with 1X PBS,
399 fixed in 4% paraformaldehyde and permeabilized with 0.25% Triton X-100 (Sigma-Aldrich
400 Inc.). After blocking (4% BSA and 4% FBS in PBS), coverslips were incubated with anti–
401 RanGTP (26915, NewEastBioscences, diluted 1:100), anti p-γ-H2AX (Ser139) (05-636, EMD
402 Millipore, diluted 1:2000), anti-Rad51 (ab213, Abcam, diluted 1:750), anti 53BP1 (NB100-305,
403 Novus Biologicals, diluted 1:2500) and anti-Geminin (10802-1-AP, Proteintech, diluted 1:1000)
404 antibodies in blocking buffer for 2 hours at room temperature. Subsequently, samples were
405 incubated with Cy-5 (1:500, Life Technologies Inc.) and Alexa Fluor 488 (for Geminin)
406 secondary antibodies for 1 hour. Coverslips were mounted onto slides using Prolong® Gold anti-
407 fade reagent with DAPI (Life Technologies Inc.). Images were obtained using a Zeiss
408 microscope (Zeiss observer Z1) with a 20X objective. For Rad51 and 53BP1 analysis, cells were
409 transfected with siRan or treated with M36 for 48 hours then gamma-irradiated at 10 Gy and
410 fixed one hour after irradiation. Automated analysis software from Zeiss (AxioVision™, Carl

411 Zeiss) was used for foci counting. In each condition, γ-H2AX, Rad51 and 53BP1 foci were
412 quantified in roughly 400 nuclei.

413 **Cellular Thermal Shift Assay (CETSA)**

414 OV1946 cells (10^7 cells/petri) were seeded in 100 mm × 15 mm petri dish and allowed to attach
415 for 24 h. Then, cells were treated with DMSO or M36 at concentrations from 50 to 200 μM and
416 incubated for 1 h at 37 °C. After incubation, cells were washed, trypsinized and centrifuged for 5
417 minutes at 1200 rpm. Cells were resuspended in HBSS, divided into different aliquots and heated
418 for three minutes at different temperatures using the Biometra TOne PCR (Analytikjena, Jena,
419 Germany). Cell lysates were then obtained by three freeze-thaw cycles in liquid nitrogen (1 min
420 each step of each cycle) followed by centrifugation at 20,000 × g for 20 min at 4°C. The
421 supernatants were harvested, and SDS-PAGE loading buffer was added before boiling for 5min.
422 Proteins were migrated and blotted into PVDF membranes. Primary antibodies used were: Ran
423 (ab53775, Abcam, 1/5000) and β-Actin (ab6276, Abcam, 1/5000). Proteins were detected by
424 HRP-secondary antibody and the ECL detection kit (Clarity and Clarity Max ECL Western
425 Blotting Substrates from Biorad). Densitometry analyses were conducted using the UV-VIS
426 Spectrophotometer (Thermo Fisher Scientific) and relative intensity of Ran protein was obtained
427 by the ratio over the β-actin band.

428 **HiBiT CETSA**

429 The cDNA of human Ran was cloned into the mammalian expression vector pcDNA3.1(+) with
430 an N-terminal HiBiT tag (from Promega) for luminescence detection. The empty pcDNA3.1(+)
431 vector was used as negative control. OV1946 cells (4 x 10^6 cells/well) cells were seeded in 6-
432 well plates. After 24 h, transfection was performed using Lipofectamine™ 3000 (Thermo Fisher
433 Scientific) according to the manufacturer's protocol. Twenty-four hours post-transfection, cells

434 were treated with DMSO (vehicle control) or 100 μM M36 for 1 h. Cells were then harvested,
435 resuspended in HBSS, and distributed into 96-well PCR plates. Samples were heated at different
436 temperatures for 3 min in a thermocycler and rapidly cooled on ice. Following heat treatment,
437 cells were lysed using the Nano-Glo® HiBiT Lytic Detection System (Promega) and incubated
438 for 10 min at room temperature. Luminescence was measured according to the manufacturer's
439 instructions. Luminescence readings were normalized to the background value of the empty
440 plasmid and to the value of the first temperature used.

441 **Ran, Cdc42, RhoA and Rac1 activation assays**

442 Cells were seeded onto 6-well tissue culture plates in such a way that cell confluence reached
443 approximately 70% the day of the experiment. The day of the experiment cells were treated for 1
444 hour with the indicated compounds prior to protein extraction and quantification. Assays were
445 performed using the Ran, Rac1 activation assay kits (Cell Biolabs) and the RhoA and Cdc42 G-
446 LISA activation assay kits (Cytoskeleton®) according to the manufacturer recommendations.

447 ***In vivo* study**

448 For the PK studies, 6-week-old female CD1 mice (Charles River laboratories, Senneville, QC,
449 Canada) received a single intraperitoneal injection of M36 (200 mg/kg), dissolved in DMSO
450 10%, Kolliphor® EL 10%, PEG-400 20% and PBS 60%. For each time point (5, 30, 120, 240,
451 360 and 1440 minutes), 3 mice were sacrificed and blood was collected by cardiac puncture.
452 Plasma levels of the compound were measured by mass spectrometry. For the tolerance test,
453 M36 was dissolved as described above and injected intraperitoneally into 6-week-old female
454 NOD.Cg-Rag1^{tm1Mom}Il2rg^{tm1Wjl}/SzJ (NRG) female mice (The Jackson laboratory, Bar Harbor,
455 ME) every day (except on weekends) at 200 mg/kg. During this study, mice were monitored for
456 survival and weight loss/gain. For the tumor xenograft experiment, NRG mice were injected with

457 10^6 TOV112D cells suspended in a mix of 1:1 PBS and matrigel (BD Biosciences) at
458 subcutaneous sites. Treatments with M36 or Olaparib started the following day. Measurements
459 of tumor size were collected at least twice a week until tumors reached limit points (2000 mm3).
460 All animal procedures were performed in accordance with the guidelines for the Care and Use of
461 Laboratory Animals of the CRCHUM and were approved by the Comité institutionnel de
462 protection des animaux (CIPA) (Protocols #C18009AMMs and C22014AMMs).

463 **Micro-dissected tissue (MDT) production, culture and treatment**

464 MDTs were obtained from both EOC cell xenografts or patient tissue samples. For the
465 xenografts, cell suspensions containing $1x10^6$ cells for TOV112D or $5x10^6$ cells for OV1946 in
466 PBS-Matrigel were injected subcutaneously in NRG female mice. Solid tumors were harvested
467 at volumes between 800 and 1500 mm^3. For patient tissue, tumor sample was collected following
468 informed consent from the Centre hospitalier de l'Université de Montréal (CHUM), Division of
469 Gynecologic Oncology. Tissue was processed immediately upon retrieval. The use of human
470 sample was approved by the Comité d'éthique de la recherche du CHUM (CÉR-CHUM, Protocol
471 #BD 04.002).

472 The micro-dissection and loading procedures were adapted from previously published work [46,69].
473 Briefly, both xenograft and patient tumor sample were sliced into 1cm slices using a scalpel and
474 processed into 350µm slices using a McIlwain™ tissue chopper (Ted Pella©). Tissue slices were
475 kept in Hank's balanced salt solution (HBSS, Wisent) supplemented with 10% FBS, 55 µg/mL
476 of gentamicin and 0.6 µg/mL of amphotericin B. A 500 µm biopsy punch (PUN0500, Zivic
477 instruments) was then used to produce MDTs, spheroidal tissue of approximately 300 µm in
478 diameter. The loading and trapping of MDTs in microfluidic devices were performed as
479 previously described [46]. MDTs were cultured in OSE (xenografts) or Ovarian TumorMACS™

480 (MILTENYI BIOTEC; patient sample) media supplemented with 10% FBS, 55 ug/mL of
481 gentamicin and 0.6 ug/mL of amphotericin B.
482 MDTs were treated with either 100 or 200 μM of M36 in 1% DMSO (Sigma) for 24 or 72hrs
483 continuously. MDTs were then fixed with 10% formalin (Chaptec) and processed following a
484 previously published paraffin-embedding lithography procedure to create micro-dissected tissue
485 microarray (MDTMA) blocks [46].

486 **MDT Immunofluorescence staining and quantification**

487 MDTMA blocks were cut into 4μm sections and put on Matsunami TOMO® hydrophilic
488 adhesion slides (VWR). Slides were stained for KI67 and cleaved-caspase 3 (CC3) to assess
489 proliferation and cell death, respectively, using the *Discovery Ultra* automated stainer (Ventana
490 Medical System inc. (VMSI)). A pan-cytokeratin (CK) antibody was also used to identify the
491 tumor epithelium of the MDTs. Slides were heated at 60˚C for 20 min before staining. Antigen
492 retrieval was carried out with Cell Conditioning 1 solution (VMSI) for 90 min. Mouse anti-KI67
493 (1:500) (9449S, Cell Signaling), rabbit anti-CC3 (1:200) (9661S, Cell Signaling) and guinea pig
494 anti-pan-CK (1:200) (BP5069, Cedarlane) antibodies were dispensed automatically and slides
495 were incubated for 60 minutes at 37˚C. Secondary antibodies, including anti-mouse Alexa 488
496 (1:250) (A-11001, Life Technologies), anti-rabbit Alexa 750 (1:200) (A-21039, Life
497 Technologies) and anti-guinea pig Alexa 647 (1:200) (706-605-148, Cedarlane) were also
498 dispensed automatically and slides were incubated for 60 minutes at 37˚C. A mounting medium
499 with DAPI (MJS Biolynx inc) was used to stain the nuclei. Slides were scanned at 20x with
500 either an Olympus BX61 (Olympus) or an Aperio Versa 200 (Leica) microscope. IF filters used
501 for DAPI, KI67, CC3 and tumor epithelium were DAPI, Alexa-488, Cy7 and Cy5, respectively.
502 Stained MDTs were quantified using the VisiomorphDP software (VisioPharm, Denmark,

503 http://visiopharm.com). Percent of CC3 staining or nuclear K-67 staining in the cytokeratin
504 positive area were quantified and plotted as bar graphs.

505 **Statistical analysis**

506 Data from at least three independent experiments are presented as the means ± SD. Statistical
507 analyses were done using GraphPad Prism version 10 (GraphPad Sofware Inc., http://
508 graphpad.com). Comparisons were carried out using Student's t-test. Analysis of MDTs was
509 done using Two-way ANOVA followed by Tukey's test. Comparisons of survival curves were
510 performed using log-rank test. A p-value of less than 0.05 was considered statistically
511 significant.

512

513 **ACKNOWLEDGMENTS**

514 We thank Kim Leclerc Désaulniers and Lise Portelance for technical assistances with the animal
515 experiments and biobank specimen procurement, respectively. We acknowledge the CRCHUM
516 animal facility, the ICM Imaging/Live Imaging platform, the Molecular Pathology core facility
517 of the CRCHUM and the CRCHUM Microfluidic platform. A-MM-M and DP are researchers of
518 the CRCHUM/ICM, which receive support from the Fonds de recherche du Québec – Santé
519 (FRQS). ZB was supported by a MITACS fellowship and by the ICM NathalieMoreau Bursary.
520 SR was supported by a studentship from the Canderel Fund of the Institut du cancer de Montréal
521 (ICM).

522

523 **FUNDING**

524 This work was supported by the Canadian Institute for Health Research (CIHR MOP142724 and
525 PJT148642), the Oncopole in collaboration with the FRQS, the Cancer Research Society,

Génome Québec and IRICoR (#265877), and the ICM (Fonds Défi Spyder and Anne-Marie Chagnon). Cell lines as well as patient tissue sample used in this study were provided by the CRCHUM ovarian tumor bank, which is supported by Ovarian Cancer Canada (OCC) and by the Banque de tissus et de données of the Réseau de recherche sur le cancer (RRCancer) of the FRQS affiliated with the Canadian Tumor Repository Network (CTRNet).

AUTHOR CONTRIBUTIONS

ZB, XT, EC, JHW and A-MM-M designed the study. ZB, XT, SR, RG and JK-D performed the experiments. ZB, XT, EC, SR, RG and JK-D analyzed the data. ZB and XT wrote the manuscript. EC, JHW, DP, and A-MM-M supervised the study, provided guidance, and edited the manuscript.

FIGURES

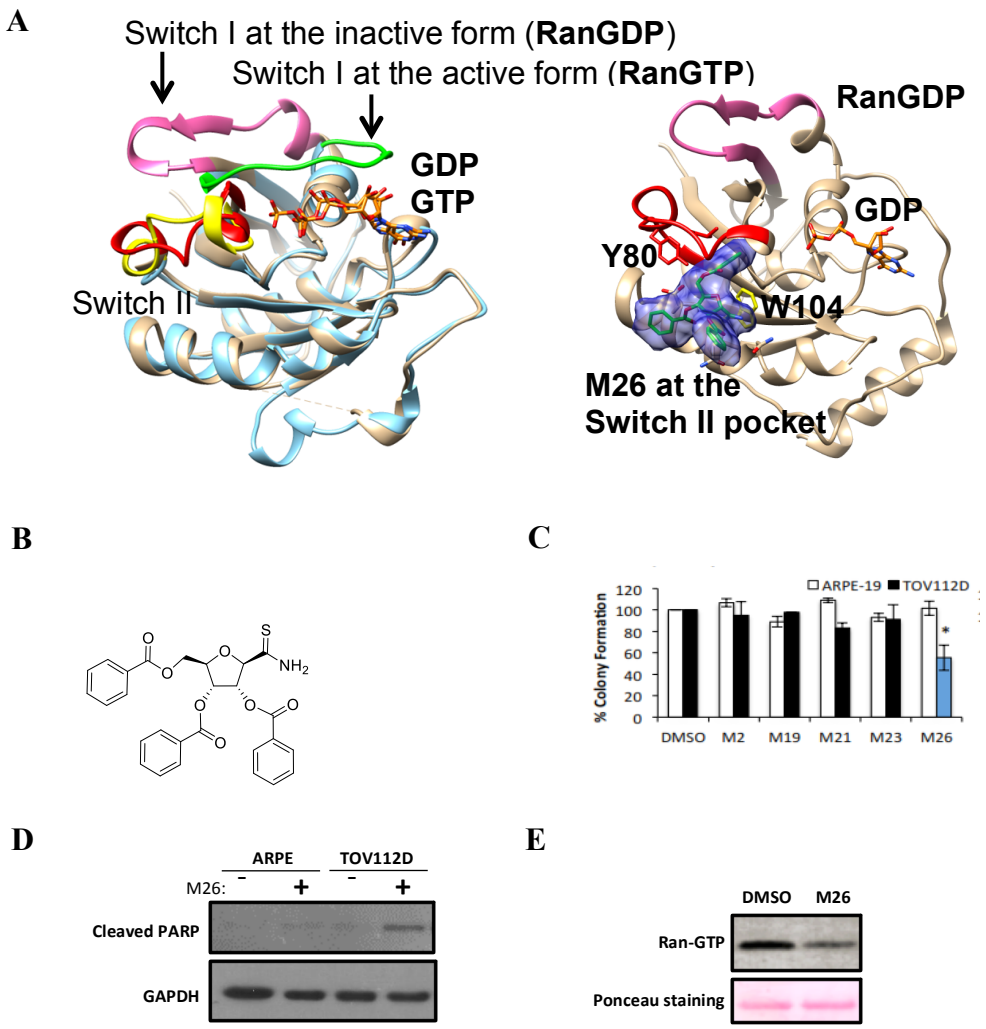

Figure 1: *In silico* and cell-based screenings identified M26 as a hit compound for Ran inhibition.

(A) Left side: Crystal structure of RanGDP (pdb: 3ch5) was aligned to RanGTP (pdb: 3nc1), showing different conformations of Switch I at the activated and inactivated states; Right side: Structural model of the switch II pocket of RanGDP was built by homology modeling and the predicted binding mode of M26 (green sticks with blue surface) at the switch II pocket of RanGDP was showed. **(B)** Chemical structure of M26. **(C)** Colony formation inhibition by selected M compounds at 10 μM in normal ARPE and EOC TOV112D cells. Only the

550 compound M26 inhibited TOV112D without affecting ARPE (blue bar). Bars represent
551 percentage of colonies formed compared to DMSO-treated controls. **(D)** ARPE and TOV112D
552 cells were incubated with M26 to evaluate apoptosis by western blot using the antibody anti-
553 cleaved PARP. **(E)** TOV112D cells were incubated for one hour with M26 (50 μM) before
554 performing RanGTP pull-down assay on the resultant cell extract.
555

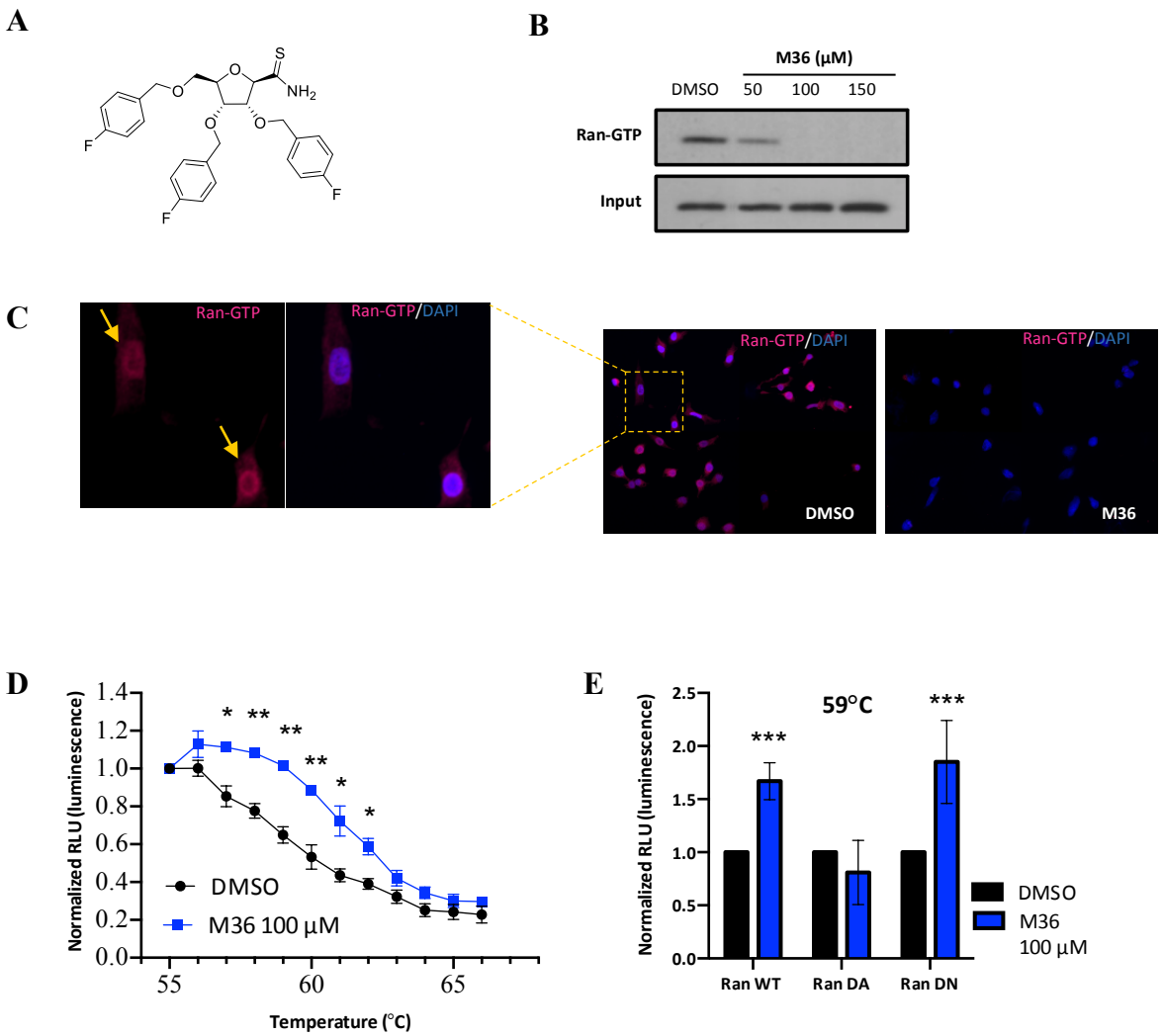

556

557 **Figure 2: M36, a derivative of M26, binds and impacts Ran activation in EOC cells**

558 **(A)** Chemical structure of M36. **(B)** TOV112D cells were treated for one hour with increasing
559 concentrations of M36. Subsequently, RanGTP pull-down assay was performed to assess Ran
560 activation. **(C)** TOV112D cells were treated with M36 (100 µM) for one hour. After cell fixation
561 and permeabilization, RanGTP was revealed by immunofluorescence using a specific antibody
562 (pink). Nuclei are shown by Dapi staining (blue). **(D)** OV1946 cells were transiently transfected
563 with Ran cDNA containing N-Terminal HiBiT or with empty plasmid, and then treated with 100
564 µM M36 (blue square symbols) or DMSO (black round symbols) for one hour (see Methods for

565 detail). Luminescence of the HiBiT tag was evaluated in cell extracts after heating the cells at
566 different temperatures for three minutes. Values represent luminescence readings normalized to
567 the background value of the empty plasmid and to the first temperature used (55°C). **(E)**
568 OV1946 cells were transiently transfected with HiBiT Ran WT or mutants dominant active
569 Ran^{Q69L} or dominant negative Ran^{T24N} and then treated with 100 μM M36 (blue bars) or DMSO
570 (black bars) for one hour. Luminescence of the HiBiT tag was evaluated in cell extracts after
571 heating the cells at 59°C for three minutes. Values represent luminescence readings normalized
572 to the DMSO treated cells. *$P < 0.05$ **$P < 0.01$ *** $P < 0.001$ (n = 3, Student's t-test).
573

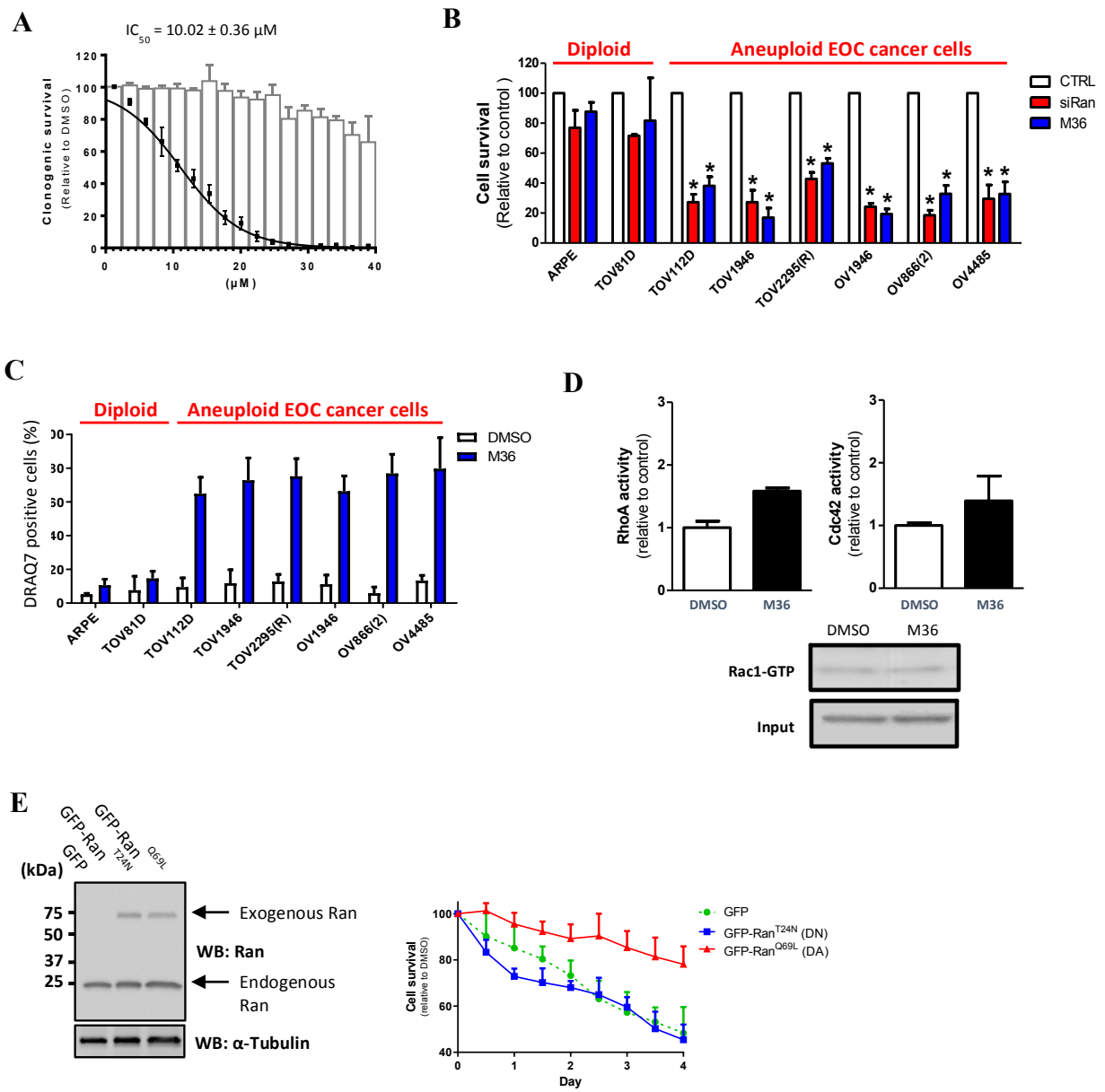

Figure 3: M36 shows selectivity for aneuploid cells and does not interferes with the activation of other GTPases.

(A) Clonogenic assay using different concentrations of M36 in ARPE and TOV112D cells. IC_{50} value was calculated for the TOV112D cells. Bars and curve points represent percentage of colonies formed compared to DMSO-treated controls in ARPE and TOV112D cells, respectively. **(B)** different EOC cell lines and the normal ARPE cells were transfected with a

581 siRNA targeting Ran or with M36 (40 μM) before assessing cell proliferation using the live cell
582 imaging IncuCyte system. Data are expressed as the percentage of control cells at the end of
583 experiment (96 h) and are representative of at least three independent experiments. **(C)** ARPE
584 and EOC cells were treated with M36 (40 μM) for 6 days and then cell death was assessed by
585 FACS using DRAQ7 staining. **(D)** TOV112D cells were treated for one hour with M36 (50 μM)
586 in order to evaluate RhoA (left), Cdc42 (right) and Rac1 (bottom) activities. **(E)** Immunoblots
587 showing successful overexpression in TOV112D cells of dominant active Ran^{Q69L} and dominant
588 negative Ran^{T24N} (left panel). These cells were treated with M36 and cell proliferation was
589 assessed using the live cell imaging IncuCyte system (right panel). Data are expressed as the
590 percentage of DMSO treated cells. *$P < 0.05$ ($n \geq 3$, Student's t-test).
591

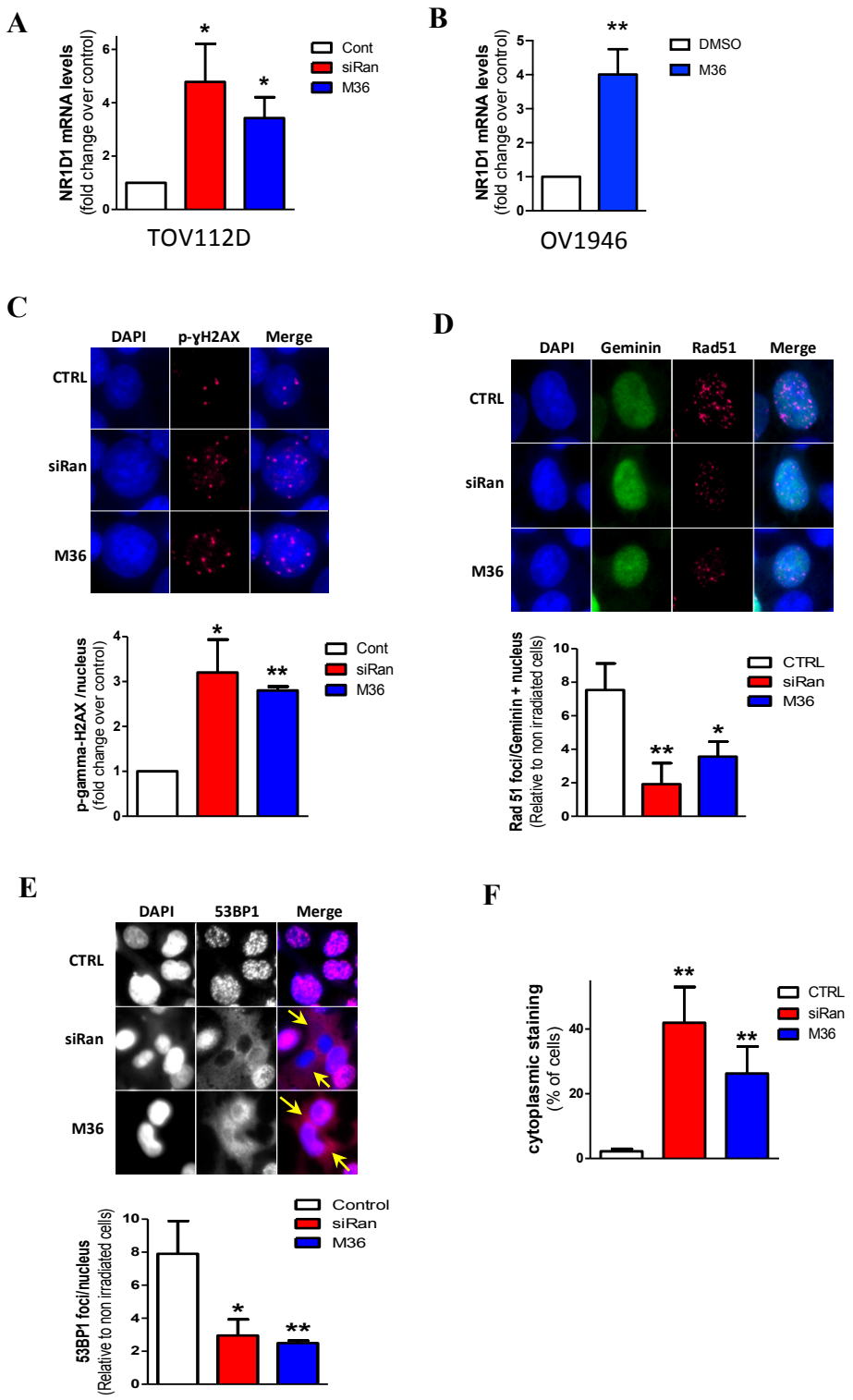

592

593 **Figure 4: M36 mimics the effect of Ran KD regarding DDR**

594 **(A)** The expression of NR1D1 was evaluated by qRT-PCR in TOV112D cells transfected with
595 siRan or treated with M36 (40 μM). **(B)** OV1946 cells were treated with M36 (50 μM) and
596 expression of NR1D1 was evaluated by qRT-PCR. **(C-E)** TOV112D cells were treated with
597 siRan or M36 (20 μM) and allowed to grow for 72 hours. For p-γH2AX staining **(C)**, cells were
598 fixed and stained. For Rad51 **(D)** and 53BP1 **(E)** staining, cells were gamma-irradiated at 10 Gy
599 and fixed 1 hour after irradiation. Representative images after irradiation **(upper panel)** and
600 quantitative analyses of foci formation **(lower panel)** are presented. For Rad51 and 53BP1 foci,
601 data are expressed as the ratio between foci number after and before irradiation. **(F)** Images
602 obtained from **(E)** were used to quantify cells presenting cytoplasmic staining of 53BP1. *$P < 0.05$ **$P < 0.01$ ($n \geq 3$, Student's t-test).
603
604

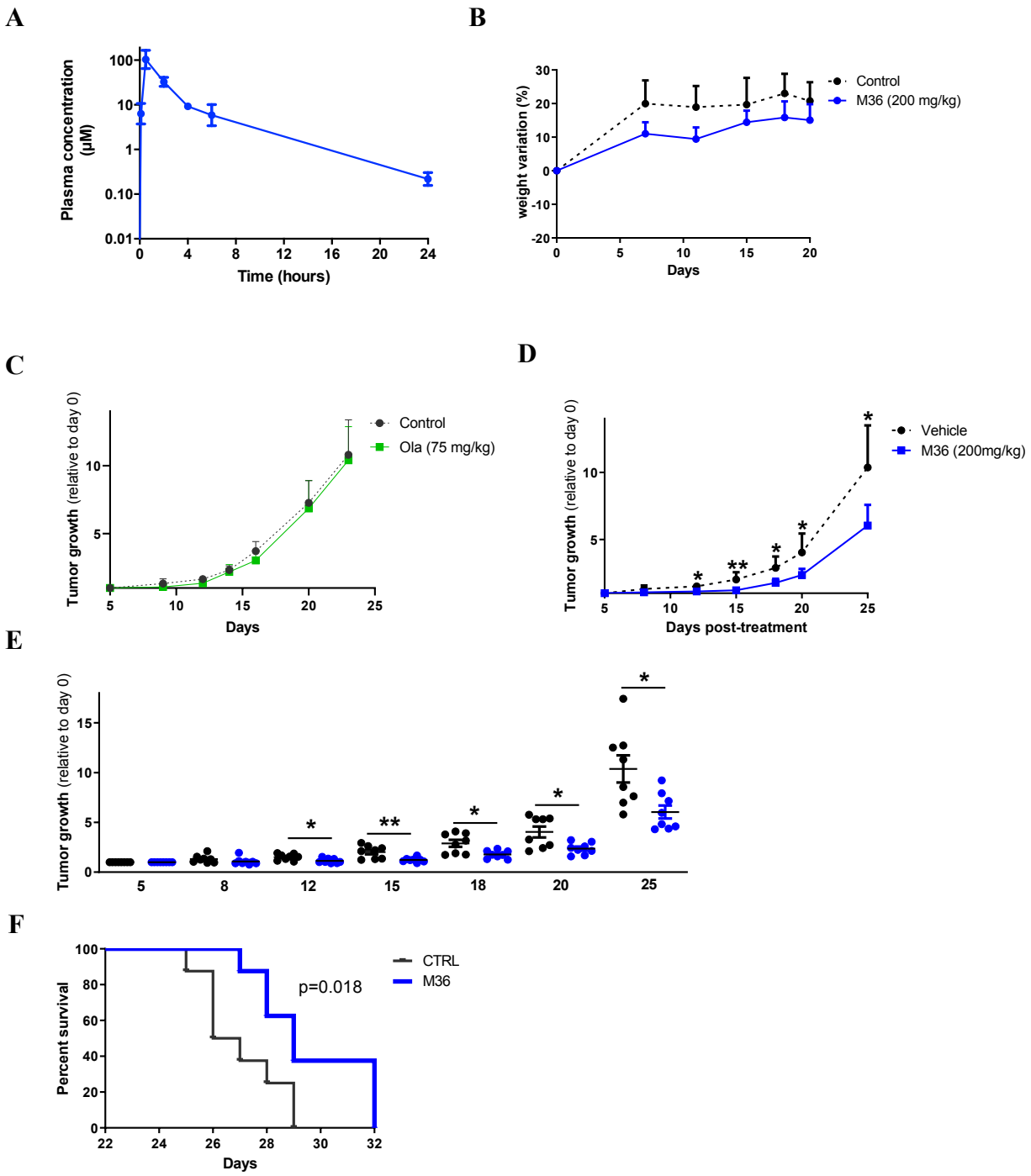

605

606 **Figure 5: Evaluation of the therapeutic potential of M36 *in vivo***

607 **(A)** Measurements of plasma levels of M36 compound after a single intraperitoneal injection

608 (200 mg/kg) in CD1 mice. **(B)** M36 (200 mg/kg) was injected IP daily in NRG mice for 3 weeks.

609 Mouse weight was measured at the indicated time points and expressed as the percentage of their
610 weight on the day of the first injection. **(C-D)** TOV112D cells were subcutaneously injected in
611 NRG mice and treatments with Olaparib (75 mg/kg, daily) **(C)**, and M36 (200 mg/kg, daily) **(D)**
612 were performed. Data are normalized with the mean of tumor size at the first day of injection.
613 **(E)** Tumor growth in individual mice treated with M36 is shown. **(F)** Kaplan-Meier survival
614 curve of mice from **(D-E)**. In **(D)** and **(E)** data were analyzed using the two-tail Student's t test.
615 In **(F)**, data were analyzed using the Log rank test. *$P < 0.05$, **$P < 0.01$.
616

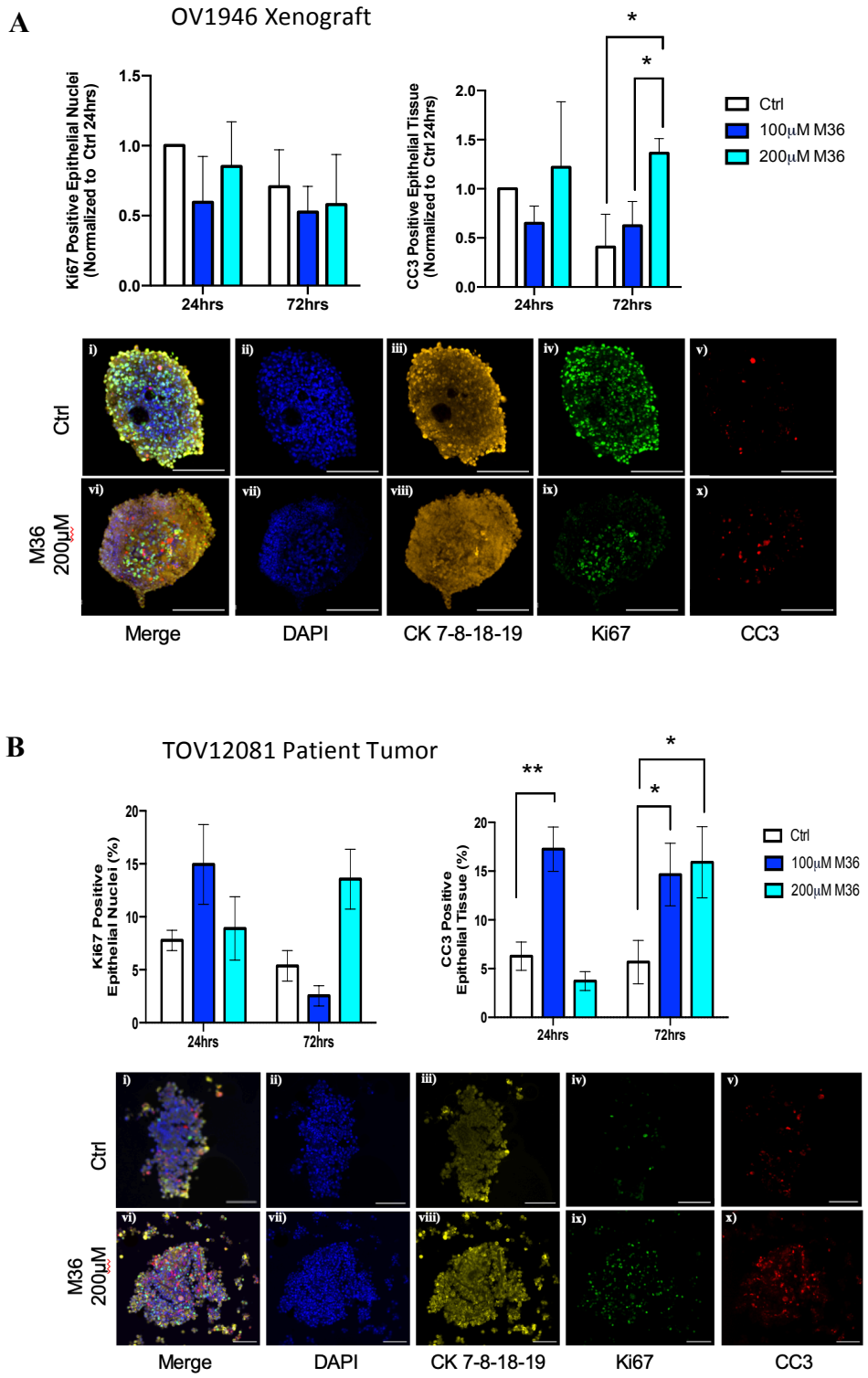

Figure 6: M36 induces cell death of *ex vivo* micro-dissected tumors from xenograft and patient tissue

620 Samples from OV1946 xenografts **(A)** or TOV12018G patient tumor **(B)** were processed as
621 micro-dissected tissues (MDTs) and cultured in microfluidic devices as described in Methods.
622 MDTs were treated with M36 at different concentrations for 24 or 72 h and then formalin-fixed,
623 paraffin embedded. Sections (6μ) were stained for KI67 (green), cleaved-caspase 3 (red), a
624 cytokeratin cocktail (yellow) and DAPI (blue). Bar graphs represent the expression of nuclear
625 KI67 (left panels) or CC3 (right panels) within the tumor epithelium (CK positive cells) of each
626 MDT. Data shown represents mean ± SEM of three separate experiments, normalized to Ctrl
627 24hrs. Statistical analysis was done using Two-way ANOVA followed by Tukey's test. *$P < 0.05$.
628 Scale bars of representative images are 200 μm.
629

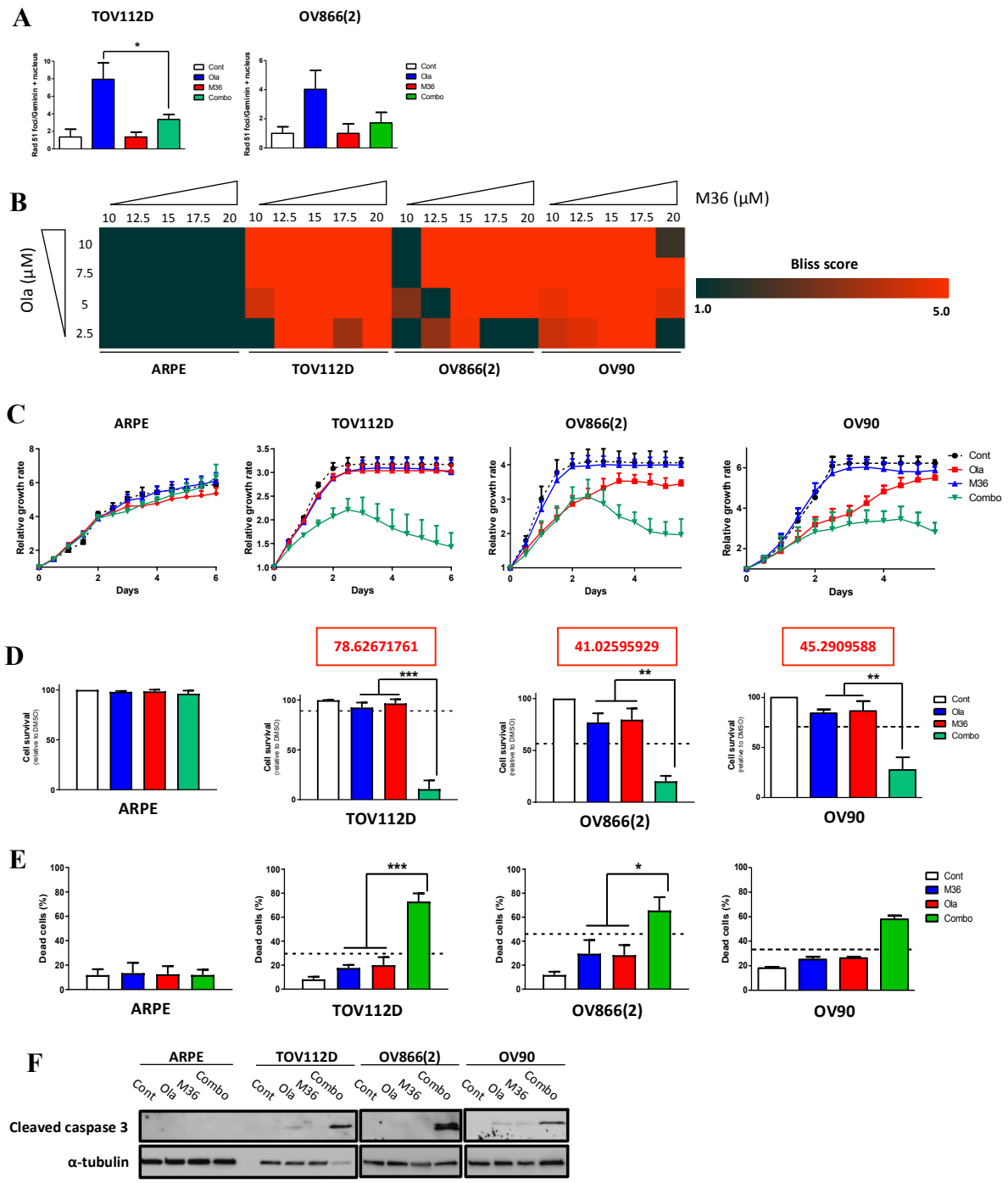

Figure 7: Combination of M36 and Olaparib triggers synthetic lethality in EOC cells

(A) TOV112D and OV866(2) cells were treated with M36 (20 µM) for 48 hours then with Olaparib (10 µM) for 24 hours. After fixation, cells were immunostained with Rad51 antibody.

634 Quantitative analyses of foci formation are presented. **(B)** Cells were treated with increasing
635 concentrations of M36 and/or Olaparib. The heat map shows Bliss scores calculated for each
636 combination at day 6. **(C)** For each cell line, an example of proliferation profile following
637 Olaparib and M36 combination treatment is presented. **(D)** At the end of the experiment
638 presented in **(C)**, dead cells were removed by PBS washes and cell confluence was measured
639 using the live cell imaging IncuCyte system. Data are expressed as the percentage of control
640 cells. **(E, F)** ARPE and EOC cells were treated as in **(C)** and apoptosis was assessed by flow
641 cytometry **(E)** and western blot **(F)** using DRAQ7 dye and cleaved caspase 3 antibody,
642 respectively. *P < 0.05 **P < 0.01 *** P < 0.001 (n = 3. Student's t-test).

643

644

645 **REFERENCES**

646 1 Matchett, K. B. *et al.* Ran GTPase in nuclear envelope formation and cancer metastasis. *Adv Exp*
647 *Med Biol* **773**, 323-351, doi:10.1007/978-1-4899-8032-8_15 (2014).
648 2 Cavazza, T. & Vernos, I. The RanGTP Pathway: From Nucleo-Cytoplasmic Transport to Spindle
649 Assembly and Beyond. *Front Cell Dev Biol* **3**, 82, doi:10.3389/fcell.2015.00082 (2015).
650 3 Azuma, K. *et al.* Ran, a small GTPase gene, encodes cytotoxic T lymphocyte (CTL) epitopes
651 capable of inducing HLA-A33-restricted and tumor-reactive CTLs in cancer patients. *Clin*
652 *Cancer Res* **10**, 6695-6702, doi:10.1158/1078-0432.CCR-04-0818 (2004).
653 4 Ouellet, V. *et al.* Tissue array analysis of expression microarray candidates identifies markers
654 associated with tumor grade and outcome in serous epithelial ovarian cancer. *Int J Cancer* **119**,
655 599-607, doi:10.1002/ijc.21902 (2006).
656 5 Ouellet, V. *et al.* Discrimination between serous low malignant potential and invasive epithelial
657 ovarian tumors using molecular profiling. *Oncogene* **24**, 4672-4687, doi:10.1038/sj.onc.1208214
658 (2005).
659 6 Abe, H. *et al.* High expression of Ran GTPase is associated with local invasion and metastasis of
660 human clear cell renal cell carcinoma. *Int J Cancer* **122**, 2391-2397, doi:10.1002/ijc.23400
661 (2008).
662 7 Xia, F., Lee, C. W. & Altieri, D. C. Tumor cell dependence on Ran-GTP-directed mitosis. *Cancer*
663 *Res* **68**, 1826-1833, doi:10.1158/0008-5472.CAN-07-5279 (2008).
664 8 Yuen, H. F. *et al.* Ran is a potential therapeutic target for cancer cells with molecular changes
665 associated with activation of the PI3K/Akt/mTORC1 and Ras/MEK/ERK pathways. *Clin Cancer*
666 *Res* **18**, 380-391, doi:10.1158/1078-0432.CCR-11-2035 (2012).
667 9 Deng, L. *et al.* Ran GTPase protein promotes metastasis and invasion in pancreatic cancer by
668 deregulating the expression of AR and CXCR4. *Cancer Biol Ther* **15**, 1087-1093,
669 doi:10.4161/cbt.29217 (2014).
670 10 Sheng, C. *et al.* Knockdown of Ran GTPase expression inhibits the proliferation and migration of
671 breast cancer cells. *Mol Med Rep* **18**, 157-168, doi:10.3892/mmr.2018.8952 (2018).

11 Boudhraa, Z., Carmona, E., Provencher, D. & Mes-Masson, A. M. Ran GTPase: A Key Player in Tumor Progression and Metastasis. *Front Cell Dev Biol* **8**, 345, doi:10.3389/fcell.2020.00345 (2020).
12 Harousseau, J. L., Shaughnessy, J., Jr. & Richardson, P. Multiple myeloma. *Hematology Am Soc Hematol Educ Program*, 237-256, doi:10.1182/asheducation-2004.1.237 (2004).
13 Hartmann, E. *et al.* Five-gene model to predict survival in mantle-cell lymphoma using frozen or formalin-fixed, paraffin-embedded tissue. *J Clin Oncol* **26**, 4966-4972, doi:10.1200/JCO.2007.12.0410 (2008).
14 Schnepp, R. W. *et al.* A LIN28B-RAN-AURKA Signaling Network Promotes Neuroblastoma Tumorigenesis. *Cancer Cell* **28**, 599-609, doi:10.1016/j.ccell.2015.09.012 (2015).
15 Cekan, P. *et al.* RCC1-dependent activation of Ran accelerates cell cycle and DNA repair, inhibiting DNA damage-induced cell senescence. *Mol Biol Cell* **27**, 1346-1357, doi:10.1091/mbc.E16-01-0025 (2016).
16 Hanahan, D. Hallmarks of Cancer: New Dimensions. *Cancer Discov* **12**, 31-46, doi:10.1158/2159-8290.CD-21-1059 (2022).
17 Yuen, H. F. *et al.* Ran GTPase promotes cancer progression via Met recepto-rmediated downstream signaling. *Oncotarget* **7**, 75854-75864, doi:10.18632/oncotarget.12420 (2016).
18 Barres, V. *et al.* An essential role for Ran GTPase in epithelial ovarian cancer cell survival. *Mol Cancer* **9**, 272, doi:10.1186/1476-4598-9-272 (2010).
19 Boudhraa, Z. *et al.* NR1D1 regulation by Ran GTPase via miR4472 identifies an essential vulnerability linked to aneuploidy in ovarian cancer. *Oncogene* **41**, 309-320, doi:10.1038/s41388-021-02082-z (2022).
20 Deng, L. *et al.* Ran GTPase protein promotes human pancreatic cancer proliferation by deregulating the expression of Survivin and cell cycle proteins. *Biochem Biophys Res Commun* **440**, 322-329, doi:10.1016/j.bbrc.2013.09.079 (2013).
21 Xia, F., Canovas, P. M., Guadagno, T. M. & Altieri, D. C. A survivin-ran complex regulates spindle formation in tumor cells. *Mol Cell Biol* **28**, 5299-5311, doi:10.1128/MCB.02039-07 (2008).
22 Torre, L. A. *et al.* Ovarian cancer statistics, 2018. *CA Cancer J Clin* **68**, 284-296, doi:10.3322/caac.21456 (2018).
23 Siegel, R. L., Miller, K. D., Fuchs, H. E. & Jemal, A. Cancer Statistics, 2021. *CA Cancer J Clin* **71**, 7-33, doi:10.3322/caac.21654 (2021).
24 Lheureux, S., Gourley, C., Vergote, I. & Oza, A. M. Epithelial ovarian cancer. *Lancet* **393**, 1240-1253, doi:10.1016/S0140-6736(18)32552-2 (2019).
25 Lheureux, S., Braunstein, M. & Oza, A. M. Epithelial ovarian cancer: Evolution of management in the era of precision medicine. *CA Cancer J Clin* **69**, 280-304, doi:10.3322/caac.21559 (2019).
26 Bashashati, A. *et al.* Distinct evolutionary trajectories of primary high-grade serous ovarian cancers revealed through spatial mutational profiling. *J Pathol* **231**, 21-34, doi:10.1002/path.4230 (2013).
27 Cancer Genome Atlas Research, N. Integrated genomic analyses of ovarian carcinoma. *Nature* **474**, 609-615, doi:10.1038/nature10166 (2011).
28 Patch, A. M. *et al.* Whole-genome characterization of chemoresistant ovarian cancer. *Nature* **521**, 489-494, doi:10.1038/nature14410 (2015).
29 Scheffzek, K., Klebe, C., Fritz-Wolf, K., Kabsch, W. & Wittinghofer, A. Crystal structure of the nuclear Ras-related protein Ran in its GDP-bound form. *Nature* **374**, 378-381, doi:10.1038/374378a0 (1995).
30 Stewart, M., Kent, H. M. & McCoy, A. J. Structural basis for molecular recognition between nuclear transport factor 2 (NTF2) and the GDP-bound form of the Ras-family GTPase Ran. *J Mol Biol* **277**, 635-646, doi:10.1006/jmbi.1997.1602 (1998).
31 Chook, Y. M. & Blobel, G. Structure of the nuclear transport complex karyopherin-beta2-Ran x GppNHp. *Nature* **399**, 230-237, doi:10.1038/20375 (1999).

723 32 Vetter, I. R., Arndt, A., Kutay, U., Gorlich, D. & Wittinghofer, A. Structural view of the Ran-
724 Importin beta interaction at 2.3 A resolution. *Cell* **97**, 635-646, doi:10.1016/s0092-
725 8674(00)80774-6 (1999).
726 33 Vetter, I. R., Nowak, C., Nishimoto, T., Kuhlmann, J. & Wittinghofer, A. Structure of a Ran-
727 binding domain complexed with Ran bound to a GTP analogue: implications for nuclear
728 transport. *Nature* **398**, 39-46, doi:10.1038/17969 (1999).
729 34 Ostrem, J. M., Peters, U., Sos, M. L., Wells, J. A. & Shokat, K. M. K-Ras(G12C) inhibitors
730 allosterically control GTP affinity and effector interactions. *Nature* **503**, 548-551,
731 doi:10.1038/nature12796 (2013).
732 35 McGregor, L. M., Jenkins, M. L., Kerwin, C., Burke, J. E. & Shokat, K. M. Expanding the Scope
733 of Electrophiles Capable of Targeting K-Ras Oncogenes. *Biochemistry* **56**, 3178-3183,
734 doi:10.1021/acs.biochem.7b00271 (2017).
735 36 Yan, C. *et al.* Discovery and characterization of small molecules that target the GTPase Ral.
736 *Nature* **515**, 443-447, doi:10.1038/nature13713 (2014).
737 37 Li, B. *et al.* Butyrylcholinesterase, paraoxonase, and albumin esterase, but not carboxylesterase,
738 are present in human plasma. *Biochem Pharmacol* **70**, 1673-1684, doi:10.1016/j.bcp.2005.09.002
739 (2005).
740 38 Martinez Molina, D. *et al.* Monitoring drug target engagement in cells and tissues using the
741 cellular thermal shift assay. *Science* **341**, 84-87, doi:10.1126/science.1233606 (2013).
742 39 Zeng, Y., Arisa, O., Peer, C. J., Fojo, A. & Figg, W. D. PARP inhibitors: A review of the
743 pharmacology, pharmacokinetics, and pharmacogenetics. *Semin Oncol* **51**, 19-24,
744 doi:10.1053/j.seminoncol.2023.09.005 (2024).
745 40 Mortison, J. D. *et al.* Rapid Evaluation of Small Molecule Cellular Target Engagement with a
746 Luminescent Thermal Shift Assay. *ACS Med Chem Lett* **12**, 1288-1294,
747 doi:10.1021/acsmedchemlett.1c00276 (2021).
748 41 Zaoui, K. *et al.* Ran promotes membrane targeting and stabilization of RhoA to orchestrate
749 ovarian cancer cell invasion. *Nat Commun* **10**, 2666, doi:10.1038/s41467-019-10570-w (2019).
750 42 Levine, M. S. *et al.* Centrosome Amplification Is Sufficient to Promote Spontaneous
751 Tumorigenesis in Mammals. *Dev Cell* **40**, 313-322 e315, doi:10.1016/j.devcel.2016.12.022
752 (2017).
753 43 Charames, G. S. & Bapat, B. Genomic instability and cancer. *Curr Mol Med* **3**, 589-596,
754 doi:10.2174/1566524033479456 (2003).
755 44 Clarke, P. R., Klebe, C., Wittinghofer, A. & Karsenti, E. Regulation of Cdc2/cyclin B activation
756 by Ran, a Ras-related GTPase. *J Cell Sci* **108 (Pt 3)**, 1217-1225, doi:10.1242/jcs.108.3.1217
757 (1995).
758 45 Brodeur, M. N. *et al.* Carboplatin response in preclinical models for ovarian cancer: comparison
759 of 2D monolayers, spheroids, ex vivo tumors and in vivo models. *Sci Rep* **11**, 18183,
760 doi:10.1038/s41598-021-97434-w (2021).
761 46 Simeone, K. *et al.* Paraffin-embedding lithography and micro-dissected tissue micro-arrays: tools
762 for biological and pharmacological analysis of ex vivo solid tumors. *Lab Chip* **19**, 693-705,
763 doi:10.1039/c8lc00982a (2019).
764 47 Lord, C. J. & Ashworth, A. BRCAness revisited. *Nat Rev Cancer* **16**, 110-120,
765 doi:10.1038/nrc.2015.21 (2016).
766 48 Bansal, M. *et al.* A community computational challenge to predict the activity of pairs of
767 compounds. *Nat Biotechnol* **32**, 1213-1222, doi:10.1038/nbt.3052 (2014).
768 49 Ly, T. K. *et al.* Activation of the Ran GTPase is subject to growth factor regulation and can give
769 rise to cellular transformation. *J Biol Chem* **285**, 5815-5826, doi:10.1074/jbc.M109.071886
770 (2010).
771 50 Kurisetty, V. V. *et al.* RAN GTPase is an effector of the invasive/metastatic phenotype induced
772 by osteopontin. *Oncogene* **27**, 7139-7149, doi:10.1038/onc.2008.325 (2008).

773 51 Yuen, H. F. *et al.* RanGTPase: a candidate for Myc-mediated cancer progression. *J Natl Cancer*
774 *Inst* **105**, 475-488, doi:10.1093/jnci/djt028 (2013).
775 52 Xia, Y. *et al.* Increased miR-203-3p and reduced miR-21-5p synergistically inhibit proliferation,
776 migration, and invasion in esophageal cancer cells. *Anticancer Drugs* **30**, 38-45,
777 doi:10.1097/CAD.0000000000000687 (2019).
778 53 Dakir, E. H. *et al.* The anti-psychotic drug pimozide is a novel chemotherapeutic for breast
779 cancer. *Oncotarget* **9**, 34889-34910, doi:10.18632/oncotarget.26175 (2018).
780 54 Anzalone, A. *et al.* Dual control of dopamine synthesis and release by presynaptic and
781 postsynaptic dopamine D2 receptors. *J Neurosci* **32**, 9023-9034, doi:10.1523/JNEUROSCI.0918-
782 12.2012 (2012).
783 55 Sharma, A., McCarron, P., Matchett, K., Hawthorne, S. & El-Tanani, M. Anti-Invasive and Anti-
784 Proliferative Effects of shRNA-Loaded Poly(Lactide-Co-Glycolide) Nanoparticles Following
785 RAN Silencing in MDA-MB231 Breast Cancer Cells. *Pharm Res* **36**, 26, doi:10.1007/s11095-
786 018-2555-6 (2018).
787 56 Haggag, Y. A. *et al.* Nano-encapsulation of a novel anti-Ran-GTPase peptide for blockade of
788 regulator of chromosome condensation 1 (RCC1) function in MDA-MB-231 breast cancer cells.
789 *Int J Pharm* **521**, 40-53, doi:10.1016/j.ijpharm.2017.02.006 (2017).
790 57 Haggag, Y. A. *et al.* Novel Ran-RCC1 Inhibitory Peptide-Loaded Nanoparticles Have Anti-
791 Cancer Efficacy In Vitro and In Vivo. *Cancers (Basel)* **11**, doi:10.3390/cancers11020222 (2019).
792 58 Desai, N. Challenges in development of nanoparticle-based therapeutics. *AAPS J* **14**, 282-295,
793 doi:10.1208/s12248-012-9339-4 (2012).
794 59 Haley, B. & Frenkel, E. Nanoparticles for drug delivery in cancer treatment. *Urol Oncol* **26**, 57-
795 64, doi:10.1016/j.urolonc.2007.03.015 (2008).
796 60 Fang, Z., Grutter, C. & Rauh, D. Strategies for the selective regulation of kinases with allosteric
797 modulators: exploiting exclusive structural features. *ACS Chem Biol* **8**, 58-70,
798 doi:10.1021/cb300663j (2013).
799 61 Kim, G. *et al.* FDA Approval Summary: Olaparib Monotherapy in Patients with Deleterious
800 Germline BRCA-Mutated Advanced Ovarian Cancer Treated with Three or More Lines of
801 Chemotherapy. *Clin Cancer Res* **21**, 4257-4261, doi:10.1158/1078-0432.CCR-15-0887 (2015).
802 62 Drean, A., Lord, C. J. & Ashworth, A. PARP inhibitor combination therapy. *Crit Rev Oncol*
803 *Hematol* **108**, 73-85, doi:10.1016/j.critrevonc.2016.10.010 (2016).
804 63 O'Malley, D. M., Krivak, T. C., Kabil, N., Munley, J. & Moore, K. N. PARP Inhibitors in
805 Ovarian Cancer: A Review. *Target Oncol* **18**, 471-503, doi:10.1007/s11523-023-00970-w (2023).
806 64 Fleury, H. *et al.* Cumulative defects in DNA repair pathways drive the PARP inhibitor response
807 in high-grade serous epithelial ovarian cancer cell lines. *Oncotarget* **8**, 40152-40168,
808 doi:10.18632/oncotarget.10308 (2017).
809 65 Ouellet, V. *et al.* Characterization of three new serous epithelial ovarian cancer cell lines. *BMC*
810 *Cancer* **8**, 152, doi:10.1186/1471-2407-8-152 (2008).
811 66 Fleury, H. *et al.* Novel high-grade serous epithelial ovarian cancer cell lines that reflect the
812 molecular diversity of both the sporadic and hereditary disease. *Genes Cancer* **6**, 378-398 (2015).
813 67 Letourneau, I. J. *et al.* Derivation and characterization of matched cell lines from primary and
814 recurrent serous ovarian cancer. *BMC Cancer* **12**, 379, doi:10.1186/1471-2407-12-379 (2012).
815 68 Provencher, D. M. *et al.* Characterization of four novel epithelial ovarian cancer cell lines. *In*
816 *Vitro Cell Dev Biol Anim* **36**, 357-361, doi:10.1290/1071-
817 2690(2000)036<0357:COFNEO>2.0.CO;2 (2000).
818 69 Astolfi, M. *et al.* Micro-dissected tumor tissues on chip: an ex vivo method for drug testing and
819 personalized therapy. *Lab Chip* **16**, 312-325, doi:10.1039/c5lc01108f (2016).

820